International Journal of Engineering, Mathematical and Physical Sciences
ISSN: 2517-9934
Vol:6, No:3, 2012

Direct Numerical Simulation of Subcooled Nucleate Pool Boiling

Sreeyuth Lal, Yohei Sato, and Bojan Niceno

***Abstract*—**With the long-term objective of Critical Heat Flux (CHF) prediction, a Direct Numerical Simulation (DNS) framework for simulation of subcooled and saturated nucleate pool boiling is developed. One case of saturated, and three cases of subcooled boiling at different subcooling levels are simulated. Grid refinement study is also reported. Both boiling and condensation phenomena can be computed simultaneously in the proposed numerical framework. Computed bubble detachment diameters of the saturated nucleate pool boiling cases agree well with the experiment. The flow structures around the growing bubble are presented and the accompanying physics is described. The relation between heat flux evolution from the heated wall and the bubble growth is studied, along with investigations of temperature distribution and flow field evolutions.

***Keywords*—**CFD, interface tracking method, phase change model, subcooled nucleate pool boiling.

I. Introduction

THE estimation of the Critical Heat Flux (CHF) has been an area of immense interest to the nuclear thermal-hydraulic community. The ability to predict CHF is important from both the safety and economics points of view. The long-term objective of our research is the prediction of high heat flux boiling and CHF within the framework of Computational Fluid Dynamics (CFD) with an interface tracking (IT) method. As the first step, we focus our attention on the low heat flux regime, in which spaced columns of bubbles originate from a limited number of pre-defined nucleation sites [1].

A number of phase change models are developed in the framework of Level Set (LS) method [2], the Volume-Of-Fluid (VOF) method [3-4], the coupled LS and VOF method [5] and the front tracking method [6]. The LS method proposed in [2] and VOF in [7] can be used to simulate nucleate boiling from a heated surface. However, the LS method is not mass conservative and a special assumption is used in [2]: the vapor inside the bubble is at the saturation temperature, T_{sat}, for the nucleate boiling, while the liquid temperature is T_{sat} for the film boiling. Due to this assumption, the phase change model proposed in [2] cannot treat transient boiling, since both nucleate and film boiling phenomena occur at the same time. In case of the VOF method in [7], the source term for the phase change is artificially smeared out and shifted across the interface using normalization factors. This smearing deteriorates the accuracy, and the shift of source term affects the temperature distribution around the shifted region.

In this paper, we present simulated flow field and heat flux of subcooled nucleate pool boiling. The phase change model proposed in [8] is used within the framework of DNS. The phase change model features a simple algorithm without any artificial assumptions; the phase change rate can be calculated from the heat flux coming at the liquid-vapor interface. The micro-region model developed by Stephan [9] is employed in it.

In Section II, the numerical method is briefly described, and the conditions of the simulation are given in Section III, followed by the results and discussions in Section IV. We wrap up the paper by conclusions given in Section V.

II. Numerical Method

A. Incompressible Navier-Stokes Equations

Viscous incompressible flows are described by the Navier-Stokes equations:

$$\frac{\partial(\rho\vec{u})}{\partial t}+\nabla\cdot(\rho\vec{u}\vec{u})=-\nabla p+\nabla\cdot\left[\mu\left(\nabla\vec{u}+(\nabla\vec{u})^{T}\right)\right]+\vec{f}\,, \tag{1}$$

$$\nabla\cdot\vec{u}=\left(\frac{1}{\rho_v}-\frac{1}{\rho_l}\right)\dot{m}\,, \tag{2}$$

where t is the time (s), ρ the density (kg/m^3), $\vec{u}$ the velocity vector (m/s), p the pressure (Pa), μ the dynamic viscosity (Pa·s), $\vec{f}$ the body force including the gravity force and the surface tension force, and $\dot{m}$ the phase change rate (kg/m^{3}s). The subscripts v and l denote vapor and liquid, respectively.

The Navier-Stokes equations are discretized with a semi-implicit projection method in time. Diffusion terms are discretized in time with the Crank-Nicolson scheme and the advection terms with the forward Euler scheme. Orthogonal finite volume method with staggered variable arrangement is used for spatial discretization. The second-order accurate central-difference scheme is used for the diffusion term and the second-order central-difference scheme for the advection term.

B. Phase Change Model

The phase change rate is defined as:

$$\dot{m}=\dot{M}\,S_{iso}/V\,, \tag{3}$$

where $\dot{M}$ is the interfacial phase change rate (kg/m^{2}s), S_{iso} the area of the interface in a cell, V the cell volume. Note that $\dot{m}$ is exactly zero for the cell which does not include interface, and thus the distribution of $\dot{m}$ can be kept sharp. The interfacial phase change rate, $\dot{M}$ is given as:

$$\dot{M}=(q_l+q_v)/L\,, \tag{4}$$

S. Lal is with the Paul Scherrer Institute, 5232 Villigen PSI, Switzerland (phone: +41-56-310-2666; fax: +41-53-310-4481; e-mail: sreeyuth.lal@psi.ch).
Y. Sato is with the Paul Scherrer Institute, 5232 Villigen PSI, Switzerland (e-mail: yohei.sato@psi.ch).
B. Niceno is with the Paul Scherrer Institute, 5232 Villigen PSI, Switzerland (e-mail: bojan.niceno@psi.ch).

where q_l and q_r are the heat fluxes reaching the interface from the liquid and the vapor phases, respectively, and L is the latent heat (J/kg). The heat fluxes q_l and q_v are defined as:

$$q_v = -\lambda_v \nabla T_v \cdot \vec{n} \ , \quad (5)$$

$$q_l = \lambda_l \nabla T_l \cdot \vec{n} \ , \quad (6)$$

where $\vec{n}$ is the normal vector of the interface, pointing from vapor to liquid phase. Second order accurate scheme is used for the discretization of ∇T in (5) and (6), preserving the accuracy of the diffusion term of the energy conservation equation.

C. Energy Equation

The energy conservation equation reads:

$$\frac{\partial}{\partial t}\left(\rho c_p T\right) + \nabla \cdot \left(\rho c_p T \vec{u}\right) = \nabla \cdot \left(\lambda \nabla T\right), \quad (7)$$

where c_p is the heat capacity (J/kgK), T the temperature (K), and λ the thermal conductivity (W/Km). The temperature of the interface between liquid and vapor is assumed to be at saturation temperature T_{sat}. In order to take the interface position into account, the irregular star method is introduced.

D. Interface Tracking Model

As an interface tracking model, the color function ϕ is introduced as the volume fraction of water inside a control volume. The interface between vapor and liquid is defined as iso-surface at $\phi = 0.5$, and the interface area as S_{iso}. The equation governing the transport of the color function reads:

$$\frac{\partial \phi}{\partial t} + \nabla \cdot \left(\phi \vec{u}\right) = -\dot{m} \frac{1}{\rho_l} \cdot \quad (8)$$

The CIP-CSL2 method [10] is used for the solution of (8), in order to achieve the exact volume conservation, and high accuracy for the advection term. To prevent smearing of the color function, the interface sharpening scheme [11] is used.

III. Conditions of Simulation

Four cases of simulation at different subcooling levels are performed: subcooling levels of 0, 1, 2, and 3 (K). The working fluid is water and steam at system pressure of 1.0 (bar). The temperature of bottom heated wall is assumed to be constant and is 6.17 (K) above the saturated temperature T_{sat}. The contact angle of the bubble at the bottom wall is assumed to be constant, and set to 38°. A nucleation site is placed at the center of the bottom heated wall. The material properties of the working fluid and the condition of the heated wall are listed in Table I.

The computational domain is a cube with an edge length of 8 mm. Three grid levels are used: a coarse grid with a minimum cell size of 0.1250 (mm), a medium grid with 0.0833 (mm) and a fine grid with 0.0625 (mm). The number of cells for each of these grids are listed in Table II.

IV. Results and Discussions

The computed flow fields for medium grid are shown in Fig. 1. Following the bubble departure, a new bubble starts to grow from the nucleation site. During the bubble growth, a strong upward flow generated by the volume expansion of the phase change is observed inside the bubble. The high temperature vapor, heated at the bottom wall, convects upward. After a certain degree of bubble growth, the neck of the bubble starts to shrink due to surface tension, eventually breaks up, and the bubble leaves the wall. The bubble departure diameter and period are 2.6 (mm) and 0.05 (s) respectively, whereas those of the experimental data reported in [2] are 2.1-2.4 (mm) and 0.025-0.033 (s). The uncertainty of the experiment is not presented in [2]. The reason for the discrepancy of the bubble departure period between the simulation and the experiment is not very clear, but it may be caused by the parameters for the micro region such as the dispersion constant.

Fig. 2 shows the computed heat flux as a function of time. The times indicated by (a) to (l) in Fig. 2, corresponds to bubble growth stages depicted in Fig. 1. When a new nucleation site is planted at (a), the heat flux increases discontinuously. The heat flux increases with growth of the bubble, and it peaks around (i), and then starts decreasing as the neck of the bubble shrinks. After the bubble departure, the heat flux reaches minimum.

Fig. 3 illustrates the grid dependent and subcooling dependent evolution of heat flux with time. Since the fine mesh represents the most accurate description of the bubble growth dynamics, we choose it for all further analysis. To analyze the subcooled pool boiling bubble growth dynamics, it is imperative to observe the growth process of a bubble under different subcooling conditions. In our analysis, a minimum of six bubble cycles are simulated for all the subcooling levels. The temperature distribution and flow-field evolutions of a particular bubble cycle are important for understanding the bubble growth dynamics. The temperature distribution and flow field evolution of the 2nd bubble cycle for subcoolings 0 and 3 (K) are given in Fig. 4 and Fig. 5 respectively, while Fig. 6 shows the temperature distribution and flow field evolution of the 6th bubble cycle for subcooling 3 (K). It can be observed from Fig. 3(a) that the mesh size has a considerable influence on the bubble growth simulation. The coarse grid results show significant over-prediction of the heat flux. However, the medium grid simulations show a good agreement with the fine mesh simulations. It can be seen from Fig. 3 (b) that as the level of sub-cooling increases, the initial heat flux at time t=0 increases. This is indeed true since with the increase in the degree of sub-cooling, the temperature difference between the heated wall and the liquid increases, as the wall temperature is assumed to be constant. The increased temperature difference leads to an enhanced heat transfer through steady state natural convection. At t=0, a new bubble seed is placed on the heated wall. At this moment, the heat flux from the wall increases rapidly as more water evaporates and the bubble size increases. The micro-region beneath the bubble plays an important role in the observed enhanced heat transfer rate. Initially, the rate of increase of heat flux, and hence the rate of bubble growth, is higher due to the larger temperature gradient. This rate of increase of the heat flux and the bubble diameter starts to decrease gradually until the peak heat flux is reached. Due to the shrinkage of the bubble neck from that point onwards, the heat flux decreases until the bubble departure. Thereafter, the evolution of heat flux follows the same cycle after a new seed is placed.

In Figs. 4-6, the velocity field is consistent with the experimental observations from [12]. At the upper part of the bubble, the vapor velocity vectors point radialy outward, while at the liquid layer beneath the bubble, the velocity vectors point

radialy inward. The bubble expansion at the bottom is countered by the friction with the heated surface as also the surface tension, both of which push the bottom part inwards. This in turn tends to push the upper portion of the bubble outwards in order to accommodate the growing vapor content inside the bubble. Two important aspects of the thermal boundary layer can be observed. In pool boiling, the thermal boundary layer plays an important role in removing the heat from the heated surface, along with the micro-layer evaporation and heat transfer by turbulent natural convection [13]. There is no noticeable thinning of the thermal boundary layer in Fig. 5, as compared to that in Fig. 4. This points to the absence of any cooling effect at the bubble-base due to the internal circulation of water which is formed due to condensation at the top of the bubble. The subcooling of 3 (K) proves to be inadequate to trigger this mechanism. In Fig. 6, the thickness of the thermal boundary layer is more than the one in Fig. 5. This is also consistent with observations in [12]. Different bubble growth processes like the increase in Nusselt number, increased heat storage in the liquid around the bubble generation site leading to a higher rate of evaporation of that part of the liquid, and the subsequent reduction of the bubble growth period, can all be traced to this increase in thickness of the thermal boundary layer with time.

Fig. 7 shows the bubble departure diameter and the bubble release period of the 6th bubble as a function of subcooling level. The departure diameter decreases and the period becomes longer as the level of subcooling increases. These tendencies agree with the experiments in [14].

In order to confirm the performance of the phase change model, the phase change rate is visualized in Fig. 8. It shows the 6th bubble of subcooling level 2 at t = 0.389 (s). The phase change occurs only around the liquid-vapor interface, owing to the sharp phase change model. Condensation is observed at the interface where the liquid temperature is less than the saturation temperature. Boiling is observed at the interface where the liquid temperature is greater than the saturation temperature. Therefore, both boiling and condensation phenomena can be simulated at the same time by the phase change model.

V. Conclusions

With the long-term objective of CHF prediction, subcooled and saturated nucleate pool boiling simulations are conducted in a DNS framework. A phase change model, which is coupled with a conservative interface tracking method, is used for the reported simulations. One saturated, and three cases of subcooled boiling at different subcooling levels are computed with a grid refinement study. Both boiling and condensation phenomena are simulated in the proposed modeling framework. The flow structure around the growing bubble is clarified with the visualization of the DNS, and the computed bubble detachment diameter of the saturated nucleate pool boiling agrees well with experiment. The relation between heat flux evolution from the heated wall and the bubble growth is studied, along with an investigation of the temperature distribution and flow field evolution.

Acknowledgment

The authors gratefully acknowledge the financial support from Swissnuclear for the project “Multi-Scale Modeling and Analysis of Convective Boiling (MSMA)”.

TABLE I
Material Properties and Condition of Heated Surface

	Water	Steam
Density ρ (kg/m^3)	9.58×10^{2}	5.79×10^{-1}
Dynamic viscosity μ (Pa.s)	2.80×10^{-4}	1.26×10^{-5}
Heat capacity c_p (J/kgK)	4.22×10^{3}	2.03×10^{3}
Thermal conductivity λ (W/m·K)	6.79×10^{-1}	2.50×10^{-2}

System pressure (bar)	1
Latent heat of evaporation L (J/kg)	2.26×10^{6}
Surface tension co-efficient σ (N/m)	5.90×10^{-2}
Wall superheat (K)	6.17
Heated surface area (mm^2)	64.0
Contact angle ($^\circ$)	38.0
Bubble seed radius (mm)	1.25×10^{-1}

TABLE II
Computational Grid

Grid	Minimum cell size (mm)	Number of cells
Coarse	0.1250	184320
Medium	0.0833	622080
Fine	0.0625	1474560

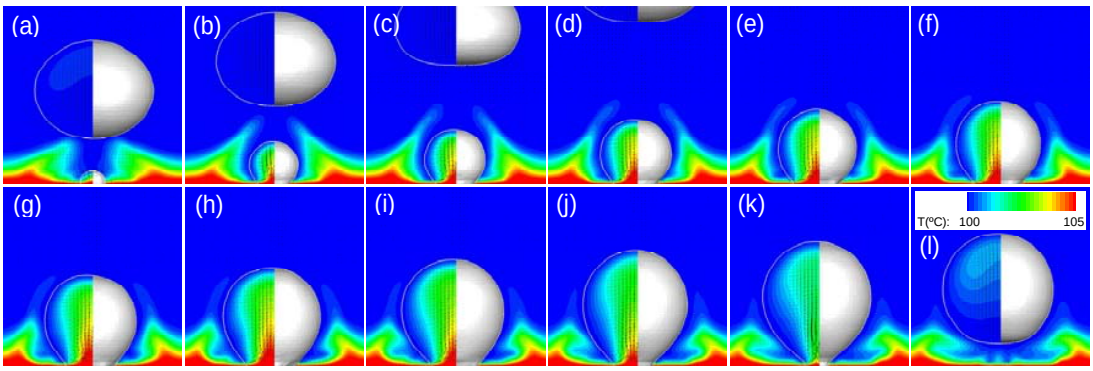

Fig. 1 Continuous saturated nucleate pool boiling from heated wall for subcooling 0 (K)

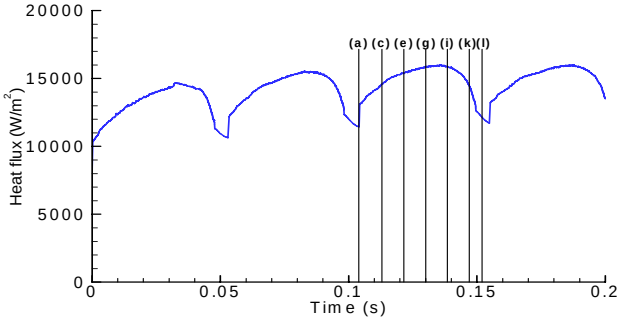

Fig. 2 Heat flux for subcooling 0 (K) as a function of time. Time indicated by (a)-(l) correspond to that of the picture depicted in Fig. 1

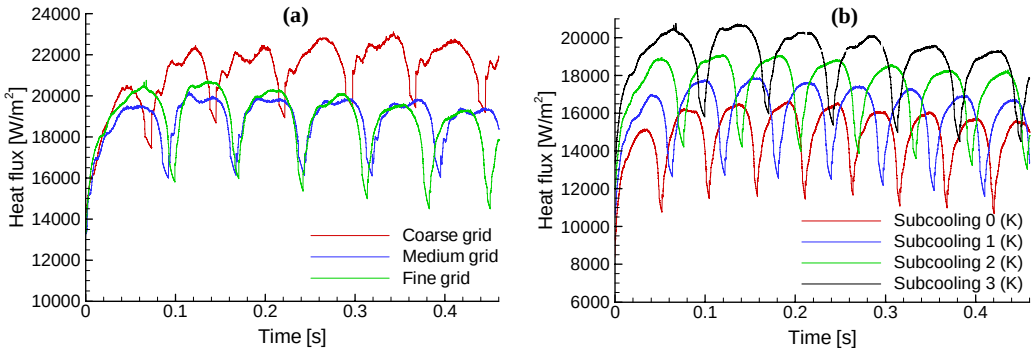

Fig. 3 Heat flux as a function of time (a) for subcooling 3 (K) for all grids and (b) for different subcoolings with fine grid

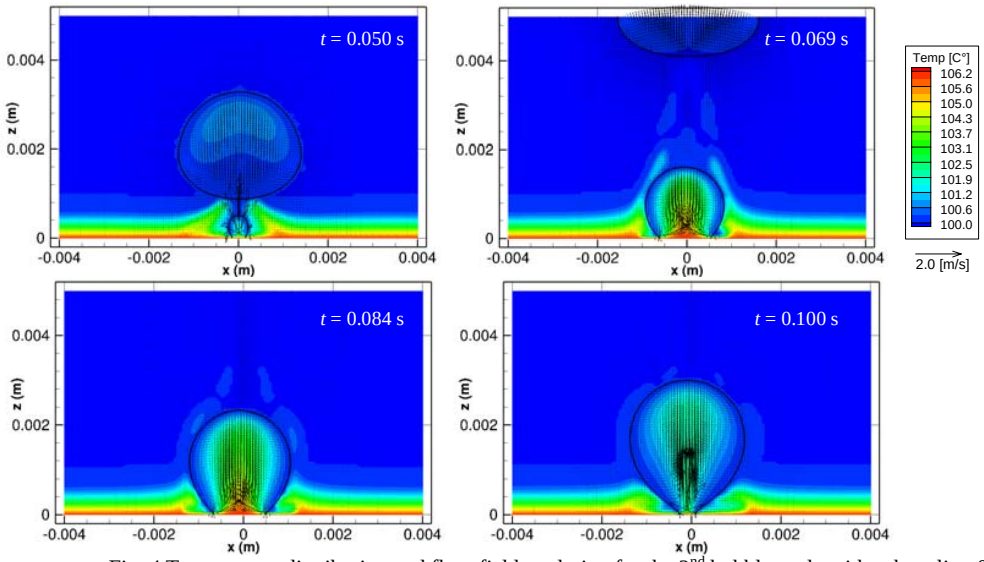

Fig. 4 Temperature distribution and flow-field evolution for the 2nd bubble cycle with subcooling 0 (K)

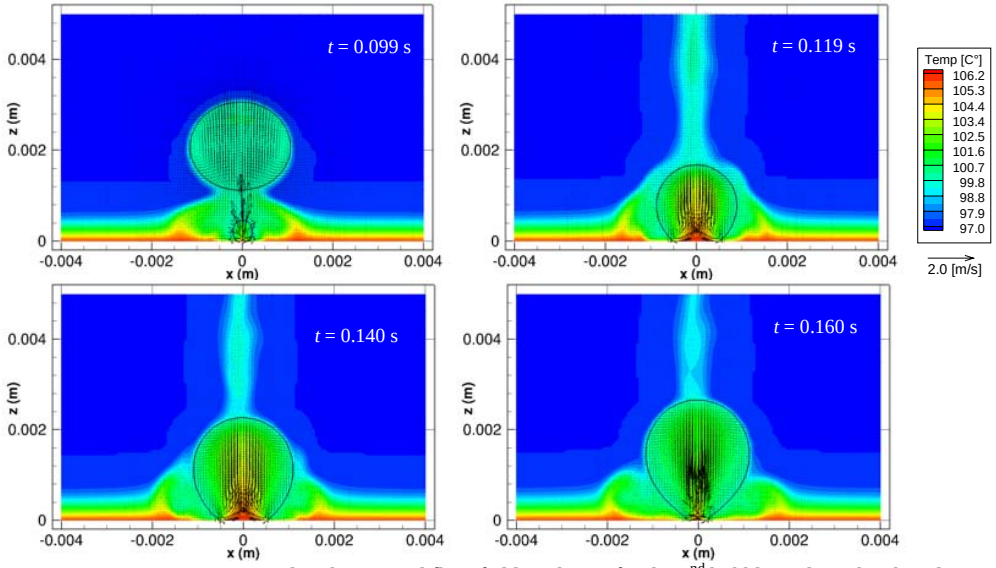

Fig. 5 Temperature distribution and flow-field evolution for the 2nd bubble cycle with subcooling 3 (K)

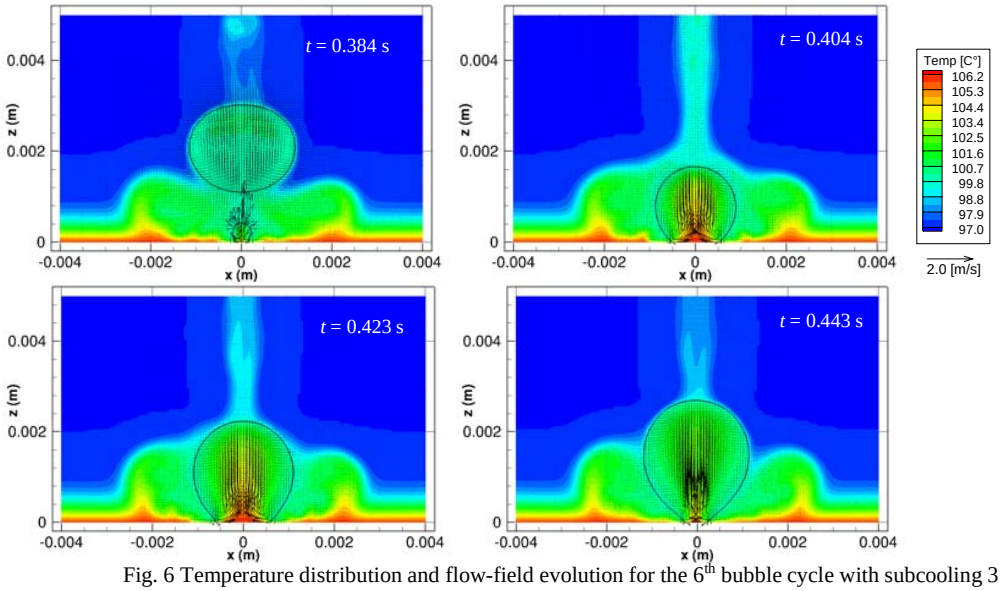

Fig. 6 Temperature distribution and flow-field evolution for the 6th bubble cycle with subcooling 3 (K)

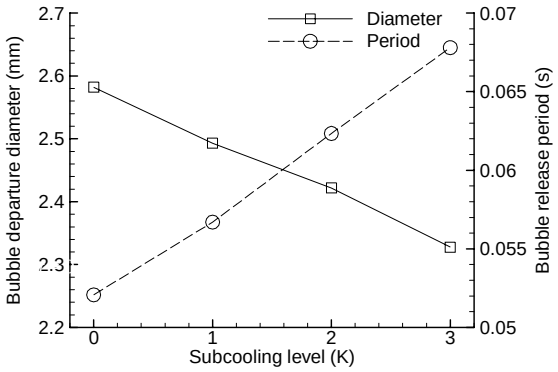

Fig. 7 Bubble departure diameter and bubble release period as a function of subcooling level

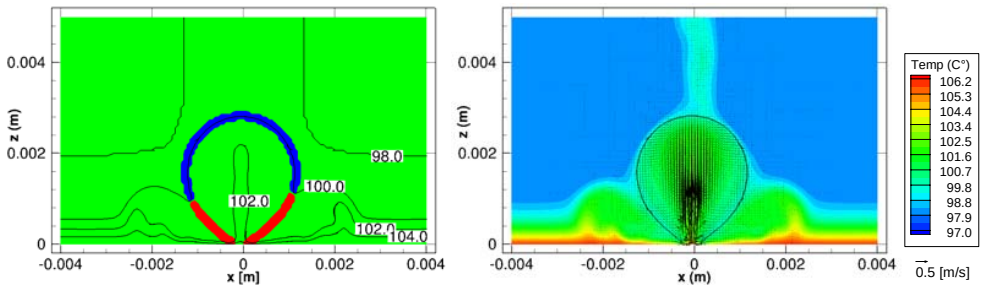

Fig. 8 Phase change rate (left) and the temperature field (right) of subcooling 2 (K) at t = 0.389 (s). In the left figure, blue indicates condensation, red indicates boiling, and the contour lines are for the temperature in unit (C°)

REFERENCES

[1] B. Niceno, Y. Sato, A. Badillo, and M. Andreani, "Multi-scale modeling and analysis of convective boiling: Towards the prediction of CHF in rod bundles," *Nuclear Engineering and Technology*, vol. 42, pp. 620-635, Dec. 2010.

[2] G. Son, V.K. Dhir, "Numerical Simulation of Film Boiling Near Critical Pressures With a Level Set Method," *J. Heat Trans.*, vol. 120, pp. 183-192, Feb. 1998.

[3] S.W. J. Welch, J. Wilson, "A Volume of Fluid Based Method for Fluid Flows with Phase Change," *J. Comput. Phys.*, vol. 160, pp. 662-682, May 2000.

[4] S. Hardt, F. Wondra, "Evaporation model for interfacial flows based on a continuum-field representation of the source terms," *J. Comput. Phys.*, vol. 227, pp. 5871-5895, May 2008.

[5] G. Tomar, G. Biswas, A. Sharma, A. Agrawal, " Numerical simulation of bubble growth in film boiling using a coupled level-set and volume-of-fluid method," *Physics of Fluids*, vol. 17, pp. 103-115, 2005.

[6] D. Juric, G. Tryggvason, "Computations of boiling flows," *Int. J. Multiphase Flow*, vol. 24, pp. 387-410, Apr. 1998.

[7] C. Kunkelmann, P. Stephan, "CFD Simulation of Boiling Flows Using the Volume-of-Fluid Method within OpenFOAM," *Numer. Heat Trans. A*, vol. 56, pp. 631 – 646, 2009.

[8] Y. Sato, B. Niceno, "A new conservative phase change model for nucleate boiling," in *Proc. 20th Int. Conf. Nuclear Energy for New Europe*, Bovec, Sep. 2011.

[9] P.C. Stephan, C.A. Busse, "Analysis of the heat transfer coefficient of grooved heat pipe evaporator walls," *Int. J. Heat Mass Trans.*, vol. 35, pp. 383-391, Feb. 1992,

[10] T. Nakamura, R. Tanaka, T. Yabe, K. Takizawa, "Exactly conservative semi-Lagrangian scheme for multi-dimensional hyperbolic equations with directional splitting technique," *J. Comput. Phys.*, vol. 174, pp. 171-207, Nov. 2001.

[11] Y. Sato, B. Niceno, "A conservative local interface sharpening scheme for the constrained interpolation profile method," *Int. J. Numer. Methods Fluids*, Avairable on early view, Oct. 2011.

[12] J. Wu and V. K. Dhir, "Numerical simulations of the dynamics and heat transfer associated with a single bubble in subcooled pool boiling," *J. Heat Transfer*, vol. 132, pp. 501-515, Nov. 2010.

[13] R. J. Benjamin and A. R. Balakrishnan, "Nucleate pool boiling heat transfer of pure liquids at low to moderate heat fluxes," *Int. J. Heat Mass Transfer*, vol. 39, pp. 2495-2504, Aug. 1996.

[14] V. P. Carey, *Liquid-vapor phase-change phenomena*, 2nd ed., London: Taylor & Francis, 2007, ch. 6.